Characterization of the retrofluorescence inhibition at the interface between glass and optically thick Cs vapor

Karine Le Bris and Jean-Marie Gagné

Laboratoire d'optique et de spectroscopie, Département de génie physique, École Polytechnique de Montréal, CP 6079, succ. Centre Ville, Montréal, Québec H3C3A7, Canada

François Babin

EXFO, 465 avenue Godin, Vanier, Québec G1M 3G7, Canada

Marie-Claude Gagné

Stocker Yale Canada, Inc., 275 Kesmark, Dollard-des-Ormeaux, Québec H9B 3J1, Canada

Received October 16, 2000; revised manuscript received May 9, 2001

New experimental results and new phenomena related to the study of the retrofluorescence spectrum induced by a diode laser at the interface between glass and cesium vapor are presented. The Cs $6^2P_{3/2}(F_e)$ hyperfine states are populated with a low-intensity tunable diode laser with a 10-MHz spectral bandwidth. We report an integrated atomic retrofluorescence spectrum in the 852.2-nm ($6^2P_{3/2}-6^2S_{1/2}$) resonance line and 917.2-nm ($6^2D_{5/2}-6^2P_{3/2}$) line generated by energy-pooling collisions. Emission spectra of the molecular fluorescence signal have been observed. At the resonance line a large proportion of the atoms excited by the laser are located in the vicinity of the surface. The interactions between the excited atomic $6^2P_{3/2}$ state and the surface appear as a spectral inhibition of the integrated retrofluorescence spectrum for both the atomic line and the molecular band. This spectral inhibition indicates that the nonradiative transformation process of changing atomically excited energy into thermal energy is preferred. We report the analysis of the dominant processes in the vicinity of the 852.2-nm resonance line, which can influence the retrofluorescence hyperfine spectrum at the boundary between the glass window and the saturated cesium vapor. Only the nonradiative transfer by evanescent waves toward the dissipative surface is retained. Using this mechanism, we formulate, for the first time to our knowledge, a simple model of a backscattered hyperfine fluorescence signal. The glass–vapor interface is considered as two distinct regions: a wavelength-thickness vapor layer joined to the surface and a more remote vapor region. The first region is analyzed as a spectral filter that annihilates the absorbed photons and the second one as a rich spectral light source. The experimental setup is described, and measured integrated retrofluorescence spectra are compared with predictions made by the model. The consistency between theory and experiment is remarkably good considering that the model depends only on two unknown parameters: the nonradiative transfer rate and the absorption shape line of the filtering region.

OCIS codes: 240.0310, 290.1350, 290.2200, 300.2530, 300.6490, 350.2450.

1. INTRODUCTION

Numerous studies have been reported for the selective-reflection phenomenon of a laser beam at the interface between a glass cell wall and an atomic vapor, optically thick at the resonance line, particularly with a metallic cesium vapor.[1–7] In all cases the internal cell surface has been considered as a dielectric substance. The possible influence of adsorbed Cs atoms on the internal surface of the glass has not been considered. However, it has recently been demonstrated that glass cell walls become electrically conductive when exposed to dry cesium vapor.[8] The surface electrical conductivity is due to a submonolayer of adsorbed cesium and a slow penetration of alkali in the glass surface underneath. This cesium adsorption transforms the glass surface into a dissipative surface with a complex dielectric constant.

The presence of a conductive glass surface near excited atoms can considerably shorten the atomic lifetime. Indeed, if the excited-atom–surface interval is a fraction of the wavelength λ, the excited atom has a higher nonradiative decay rate compared with that of spontaneous emission. These interactions generate an energy-transfer process from the excited atom toward the surface, while conserving the laser excitation population rate of the atoms. The excited atom, coupled by atomic evanescent waves with the surface, can be considered as an elementary transformer of photonic energy into thermal energy. This effect is observed without migration of excited atoms and excited atomic reflection with the surface. High-resolution spectral studies of the fluorescence spectrum should show this coupling as a dip at the line center due to photonic annihilation.

We analyzed the spectral properties of laser-interface effects using the retrofluorescence (or backscattered fluo-

rescence) method. This technique consists of observing the light emitted at the boundary by excited atoms in the direction opposite the laser beam. As the vapor is optically thick, its optical depth strongly depends on the incident laser frequency. Very near zero detuning at a resonance line, only the atoms flying very close to the surface will be able to interact with the laser. While varying the laser frequency, we should observe the nonradiativephenomena due to the surface interactions. The spectral study of retrofluorescence or backscattered fluorescence at high spectral resolution should allow us to characterize phenomena that selective-reflection spectroscopy cannot see. Indeed, unlike retrofluorescence, selective reflection entails only an instantaneous interaction between the laser radiation and the atoms near the surface. The nonradiative energy transfer of excited atoms has no observable influence on the selective reflected radiation because this process destroys the coherence between incident and emission waves.

Retrofluorescence radiation is complicated and, unlike selective reflection, has not generated much research to date. Mathematical models to describe the combined effects of radiation and migration of excitation have been used to evaluate backscattered fluorescence in the vapor–window interface for Na.[9] Nevertheless, as we see below, it is difficult to find consistency between their theory and experiment, particularly at the near-zero detuning line center, which is the spectral region most sensitive and significant for the surface effects.

In the model we are developing, the glass–vapor boundary is considered as two distinct regions: a wavelength-thickness vapor layer joined to the conductive-glass surface and a more remote atomic-vapor region. The first region is analyzed as a spectral filter dissipating photons. The fraction of the incident laser intensity that passes through the filter region is totally absorbed in the second infinitely extended region. This region becomes a secondary observable light source in the direction opposite the laser beam. This light source gives us spectral information from the glass–vapor interface.

The purpose of this paper is to present a spectral study of laser retrofluorescence at the glass-surface-cell–cesium-vapor interface. We begin with a discussion of the energy-transfer mechanisms at the boundary, followed by a phenomenon-based interpretation of the spectral effects on the backscattered-fluorescence signal. A selective and dissipative spectral optical filtering effect is proposed in order to characterize the dissipative surface effects on the retrofluorescence spectrum. The experimental setup is described, and our model is compared with experimental results.

2. ENERGY TRANSFERS AT A GLASS–CESIUM-VAPOR INTERFACE

Understanding the atomic energy losses at the interface between alkaline vapor and the dielectric boundary is essential. However, many complex processes that are hard to analyze quantitatively must be solved. In the present case, we know that the unique origin of the integrated backscattered fluorescence from the interface is produced by the laser-beam absorption and by backward spontaneous-emission resonance line $6^2P_{3/2}$–$6^2S_{1/2}$. Our objective is to show that the atomic emission of evanescent photons toward the electrical-conductivity surface of a glass cell is the principal process of energy loss at the center of the spectral resonance line.

We first specify the principal processes that can influence the backscattered-fluorescence spectrum: self-absorption and specular and diffuse collisions of the excited atoms with the surface of window. After this, we summarize the theory of lifetime-excited atoms in the presence of a conducting surface[10] or a thin conductive absorber.[11] We then provide a physical and geometric description of the glass–vapor interface.

A. Self-Absorption

Self-absorption, the phenomenon of absorption of the light emitted by an atom, can produce a self-reversal in the center of a line emerging from the light source. This phenomenon has been studied by various authors, such as Hummer *et al.*,[12] Molish *et al.*,[13] and Cowan *et al.*[14] One of the most common examples of self-reversal consists of a bright central core surrounded by a less luminous envelope. Because there are more atoms in the excited state in the hot core than in the cold envelope, the core becomes an emitter and the envelope an absorber.

In our case the self-absorption process cannot justify the retrofluorescence inhibition for two reasons. First, it is clear that the radiation emitted by atoms close to the surface can escape more easily than that emitted by atoms in the deepest layer of the cell. Because the proportion of atoms excited close to the surface increases as we tune the incident waves close to the center of the resonance line, self-absorption is minimum at resonance. This is contrary to what happens in conventional fluorescence spectroscopy by transmission. The second reason for rejecting self-absorption is experimental. If the decrease of a signal is due to self-absorption, there should not be a decrease of the signal in the transitions excited by the energy-pooling effect (inelastic collisions between excited atoms), the medium being optically thin for these transitions. Section 5 shows that the inhibition of the resonant-line signal also affects all the other transitions.

B. Surface-Quenching Phenomenon and Nonradiative Quantum Transfer

Hummer *et al.*[12] have developed a mathematical model to describe the combined effects of radiation and migration of excitation transfer. From this model the excitation is carried through the gas by a succession of atoms that experience resonant excitation exchanges; the excitation thus appears to walk randomly through the medium. The model is based on the idea that an excited atom travels in a straight line until it transfers its excitation to a nearby ground-state atom, which then carries the excitation in another random direction. This process is repeated until the excitation is quenched or converted into a real photon. In our case it must become a backscattered photon. The migration is characterized by a mean-velocity parameter. The model equations are formulated

for a plane-parallel slab of gas that is excited both by external radiation falling on one face and by internal thermal sources. Our case does not have internal thermal sources. Hummer *et al.* consider an isothermal gas of two-level atoms in the slab illuminated uniformly on one side by a collimated beam of radiation with prescribed frequency dependence. Their approach is to write separate equations for radiative transfer and transport for excited atoms. To complete the definition of the problem, the boundary conditions are specified in terms of reflection coefficients Rr and Ra for radiation and excited atoms, respectively. They note that if the mean speed $\bar{v}$ of velocity distribution is $\bar{v} = 0$, the reflection coefficient Ra drops out of the equation, as expected.

Zajonc *et al.*[9] have used this previous theory to describe the intensity of scattered radiation in a situation where losses to the boundary are significant. They have made detailed comparisons between experimental results and the solution of the equations for the transport processes. The authors suppose that their measurements show the effect of nonradiative losses at a gas–window interface. No hyperfine structure has been observed in their experimental research; only results for the fine structure of the Na spectrum have been presented. It is not clear to us why they have not observed the large hyperfine structure associated with the ground level (1.77 GHz), the line width of their laser beam being approximately 200 MHz. Nor is it clear why the adjustment between theory and experiment is significantly better for $3^2P_{3/2}$ excitation than for $3^2P_{1/2}$ excitation. From their experimental research, it is difficult to conclude that they have consistency between theory and experiment, particularly at the line center, which is the region most sensitive to boundary effects.

Zajonc *et al.* assume complete destruction of the excited atoms at the window. However, it is not possible to lower the calculated intensities at the line center by changing the reflection coefficient for the excited atom. As in the case of selective-reflection spectroscopy, they have used a reflection coefficient Ra for excited atom on the wall of the cell with a value to be contained between $0 \leqslant Ra \leqslant 1$. The nature of this strange reflection coefficient at the glass boundary cell is unknown. Schurmans[7] said "We have no precise information on the nature of the solid wall and of the atom–wall collision." Even if each atom striking the surface loses its internal energy, the loss rate cannot exceed, in a crude approximation, 1/6 of the energy of excited atoms (corresponding to the proportion of atoms going toward the surface). We observe that energetic losses are much higher than this rate.

When the laser beam is tuned to the atomic line center, resonant atoms are only those that have no velocity component in the direction of the laser beam. If the Doppler effect is dominant, the absorption process of the energy laser is confined to a very thin vapor layer (λ) adjacent to the window, and there is no quenching of excited atoms by collision with the window surface. The excited atoms remain close to the surface during their radiative lifetime. The authors do not discuss the absence of any quenching collision with the surface. It is not clear how we can use the theory without atomic collision with the surface, particularly in the region where we need the most efficiency of the surface effects. In their paper the authors do not consider that the symmetry of space velocity is broken by solid surface $\bar{v}_x^2 \neq 1/3\bar{v}^2$ for excited atoms.

Unlike Zajonc *et al.*,[9] we do not see an effect on fluorescence intensity of nonradiative excitation transport to a boundary. More extended analysis of the retrofluorescence is necessary to clarify the basic discrepancies between theory and experiment.

C. Nonraditive Energy Transfer without Collisions with Surface

Wylie *et al.*[10] have studied the behavior of an excited atom in a half-space of a vacuum bounded by a surface. They have made calculations for several properties of boundaries: perfect conductor, metallic, and dielectric. The only case that corresponds to our objective involves the interaction between an excited atom and a surface with metallic properties. Indeed, in this particular case, they noticed that the lifetime of an excited atom above a metal surface was proportional to x^{-3}, the distance between the excited atom and the surface. From their theory the rates of decay over a metal show a divergence as $x \rightarrow 0$, which is not present for a perfect conductor. The dissipation in the metal will cause the image dipole to have a component out of phase with the real dipole and therefore to be out of phase with the near field of the dipole. The dissipation occurring near the surface provides a decay mechanism for the excited atom. The divergence exists for any kind of surface with dissipation and therefore a complex dielectric constant. Based on these results, when the interval between an excited atom and the surface becomes smaller than a wavelength, we assume than the preceding decay mechanism is larger than the spontaneous-emission rate. We can understand this through the classic interpretation of the theory developed by Chance *et al.*[11] They consider the general problem of the transfer of energy from an excited atom to a metal or a dielectric. The energy transfer is considered from the viewpoint of classical electromagnetic theory. They extend the theory to treat partially absorbing surfaces of finite thickness. It is demonstrated that a thin layer (film) of an absorbing medium can produce a greater energy-transfer rate than a thicker film. There is an optimum film thickness that maximizes the transfer rate. According to these authors, the nonradiative energy transfer results from coupling of the near field of the dipole to the surface-plasmon modes in the metallic absorber. Chao *et al.*[15] in their study of cesium adsorption on a cold Si surface determined the plasmon energy in the spectral domain of a few eV: 1.0, 2.2, and 3.2. With the excited state $6^2P_{3/2}$ for cesium having energy of 1.45 eV, the plasmic coupling can be weak. Nevertheless, the surface, which is partially covered and doped by cesium, can have a dominant nonradiative energy dissipation rate.

We were concerned about the influence that a submonolayer of adsorbed cesium might have over the transfer of the laser-beam intensity and the radiance from the vapor through the cell surface. Smith[16] in 1970 has shown that a cesium film has an optical conductivity that is maximal in the near-IR. Nevertheless, the bandwidth of the cesium optical conductivity is sufficiently wide for the absorption of the incident laser beam to induce only a reduction of flux independently of the frequency.

D. Physical and Geometric Description of the Vapor–Window Interface

As stated above, backscattered fluorescence can show the interaction between excited atoms and the surface. This interaction is manifested by a nonradiative transfer of the internal energy of the atom to the surface. This transfer becomes predominant when the atom is close to the wall. It does not necessitate collision with the surface, so it is efficient whatever the motion of atoms. Thus, to simplify, we neglect the motion of the excited atoms except as it affects the absorption and emission profile by the Doppler effect.

Figure 1 is a schematic description of the characteristic region of the interface cell. A substantial amount of the Cs is adsorbed inside and on the glass surface (a).[8] Between this structure and the reservoir of cesium vapor, we must consider a so-called near-field region (b) of dimensions of the order of the wavelength (852.2 nm). In this wavelength-thickness layer the atomic evanescent waves of the atomic $6^2P_{3/2}$ dipoles are strongly coupled with the metallic nanostructure surface. This close-field region, the proximity region, contains a great number of atoms (10^{11} at. cm^{-2}) at the ground state that are spread out uniformly over the volume. The surface and the atoms localized in the near-field region constitute an efficient selective dissipative-frequency environment with maximum dissipation at the center resonance line. This arrangement and interrelationship is described as a frequency-dissipative optical filter, which partially stops the frequencies included in a bandwidth centered in the resonance lines. The filter irreversibly transforms the energy of the laser beam into thermal energy. We assume, in the first approximation, that each laser photon absorbed by an atom located in this region is transformed into thermal energy.

Adjacent to the filter structure, there are infinitely extended free atoms that we call the far-field region (c). In this region, excited atoms do not or hardly interact with the surface. It is especially in this region that the coherent laser beam is transformed into incoherent backscattered fluorescence. The far-field region therefore becomes a secondary light source observable by the window in the opposite direction with respect to the laser beam. The cesium reservoir also assumes the role of a thermostat, particularly for the population of the ground hyperfine levels. In Section 3 a simple mathematical model is developed for the backscattered-fluorescence spectrum expressed in term of the combined effect of near-field and far-field regions.

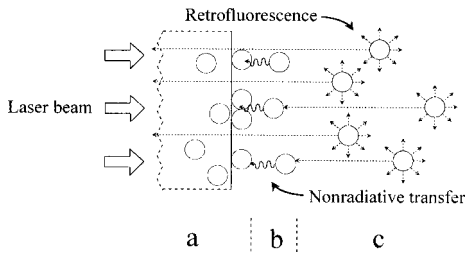

Fig. 1. Physical and geometric description of the characteristic regions of the cell: (a) metallic nanostructure surface; (b) proximity region of the surface (<λ), or near-field region; (c) far-field region where the fluorescence is generated. The regions are not to scale.

3. FORMULATION OF SIMPLE MATHEMATICAL MODEL OF THE BACKSCATTERED FLUORESCENCE

In formulating our model we begin with the basic equation for integrated retrofluorescence for atomic transition between two degenerated levels. A simple equation for the stop-band filter is considered. We see that the intensity of inhibition at a given frequency depends on the effective nonradiative transfer rate. A theoretical model of integrated retrofluorescence intensity as a function of laser tuning is presented for different values of optical thickness of the filter region at the line center. This simple model of retrofluorescence is generalized in Subsection 3.B to a more realistic atom considering the hyperfine structure for the transition $Cs[6^2S_{1/2}(F_g) \rightarrow 6^2P_{3/2}(F_e)]$.

A. Integrated Retrofluorescence in a Simple Case of an Atomic Two-Level Transition

The purpose of this subsection is to present a simple model of the retrofluorescence signal at the glass–atomic-vapor interface. We analyze the evolution of a weak, parallel, monochromatic laser through the near- and far-field regions of the interface. To simplify the formulation, we neglect reflection, absorption, and scattering of the energy laser beam in the glass window and on the surface of the cell partially covered and doped by adsorbed cesium atoms. The intensity of laser beam F_{ν_L} is weak enough that the number of excited atoms $|e\rangle$ is very much less than the number remaining in the ground state $|g\rangle$.

1. *Basic Equation for the Stop-Band Filter*

The incident radiation at the frequency ν_L absorbed in a thin atomic-layer vapor associated with the filter is found to be

$$\Delta F(\nu_L) = F_{\nu_L}\{1 - \exp[-\overline{\tau^f_{ge}}(\nu_L)]\}, \tag{1}$$

where $\overline{\tau^f_{ge}}(\nu_L)$ is the effective spectral optical thickness of the stop-band filter, for the atomic transition between the ground level $|g\rangle$ and the excited level $|e\rangle$. The value {..} is defined as the spectral absorption of the filter.

We assume that the densities of the atoms in the ground and excited levels are constant throughout the cell. $\overline{\tau^f_{ge}}(\nu_L)$ can be written as a function of the effective spectral-absorption coefficient $\overline{k^f_{ge}}(\nu_L)$ of the saturated vapor located in the near-field region:

$$\overline{\tau^f_{ge}}(\nu_L) = \overline{k^f_{ge}}(\nu_L)\overline{x_f}. \tag{2}$$

$\overline{x_f}$ is the mean geometrical depth of the near-field region (≈λ). We express $\overline{k^f_{ge}}(\nu_L)$ by using the effective spectral-absorption cross section per atom in the near-field region $\sigma^f_{ge}(\nu_L)$ and $\overline{n_g}$, the mean number density of the ground level for a temperature T:

$$\overline{k^f_{ge}}(\nu_L) = \sigma^f_{ge}(\nu_L)\overline{n_g}. \tag{3}$$

$\sigma^f_{ge}(\nu_L)$ is a function of the atomic parameter,[17]

$$\sigma^f_{ge}(\nu_L) = \frac{\lambda^2}{8\pi}\frac{(2J_e + 1)}{(2J_g + 1)}A^f_{eg}\alpha^f_{ge}(\nu_L), \tag{4}$$

where $\alpha_{ge}^{f}(\nu_L)$ is the normalized emission line shape and $\overline{n_g}$ is a well-known function of T.[18] A_{eg}^{f} is the nonradiative transfer rate in the sense that

$$A_{eg}^{f} = \epsilon_{eg} A_{eg}, \tag{5}$$

where A_{eg} is the Einstein coefficient in vacuum of the spontaneous emission between two degenerated levels whose statistical weights are $(2J_e + 1)$ and $(2J_g + 1)$, and ϵ_{eg} is the ratio between nonradiative and radiative transfer rates for a transition e–g.

So

$$\overline{\tau_{ge}^{f}}(\nu_L) = \frac{\lambda^2}{8\pi} \frac{(2J_e + 1)}{(2J_g + 1)} A_{eg}^{f} \overline{n_g} \alpha_{ge}^{f}(\nu_L) \overline{x_f}. \tag{6}$$

Thus it is necessary to know the temperature, the atomic parameters of the gas, and the effective optical depth of the filter in order to calculate the ratio ϵ_{eg}.

2. Retrofluorescence Signal

Without surface effect. The rate of energy dissipated in an elementary slice of vapor of thickness dx located at a distance x from the entrance window is described by the equation

$$\mathrm{d}F_x(\nu_L) = -F_{\nu_L} k_{ge}(\nu_L) \exp[-k_{ge}(\nu_L)x] dx, \tag{7}$$

where $k_{ge}(\nu_L)$ is the effective spectral-absorption coefficient. The exponential takes into account the intensity of laser-beam absorption on the x interval. The above equation expresses the excitation rate of the population level $|e\rangle$. Only a fraction of these excited atoms contribute to the integrated backscattered-fluorescence signal. The spectral radiance at x in the opposite direction $-\mathbf{n}_L$ due to the elementary volume dx is found to be

$$\mathrm{d}^2 L_{\nu,x}(\nu_L) = \mathrm{d}F_x(\nu_L) P_{eg}(\nu, \nu_L, -\mathbf{n}_L). \tag{8}$$

$P_{eg}(\nu, \nu_L, -\mathbf{n}_L)$ represents the conditional probability of a spontaneous-emission photon of frequency ν in the opposite direction. The conditional probability can be developed as the product of two functions:

$$P_{eg}(\nu, \nu_L, -\mathbf{n}_L) = \Gamma(-\mathbf{n}_L) r_{eg}(\nu, \nu_L), \tag{9}$$

where $\Gamma(-\mathbf{n}_L)$ is a function characterizing the spatial backward direction of emission photon and $r_{eg}(\nu, \nu_L)$ describes the frequential distribution of the emission photon. If we have a complete redistribution of the population, $r_{eg}(\nu, \nu_L)$ is taken equal to the product of quantum yield Y_{eg} by the normalized emission profile $\alpha_{eg}(\nu)$. We obtain

$$r_{eg}(\nu, \nu_L) = Y_{eg} \alpha_{eg}(\nu). \tag{10}$$

Considering that we wish to develop a simple mathematical model, we disregard multiple photonic trapping, but quenching of excited atoms by collisions and the self-absorption process are retained. So, the backscattered-fluorescence radiance due to an elementary layer dx of excited atoms by a monochromatic laser beam without surface effects is given by

$$\mathrm{d}^2 L_{\nu,x}(\nu_L) = F_{\nu_L} Y_{eg} \Gamma(-\mathbf{n}_L) k_{ge}(\nu_L) \alpha_{eg}(\nu) \times \exp\{-[k_{ge}(\nu_L) + k_{ge}(\nu)]x\} \mathrm{d}x. \tag{11}$$

The solution of this equation, by integrating over $0 < x \leqslant \infty$ and the spectral domain $\Delta\nu$, gives the observed integrated radiance of the backscattered fluorescence:

$$L_{eg}(\nu_L) = F_{\nu_L} Y_{eg} \Gamma(-\mathbf{n}_L) \alpha_{ge}(\nu_L) \int_{\Delta\nu} \frac{\alpha_{eg}(\nu)}{\alpha_{ge}(\nu_L) + \alpha_{ge}(\nu)} \mathrm{d}\nu. \tag{12}$$

It is evident from this formula that self-absorption cannot give a satisfactory interpretation of the inhibition of the radiance.

With surface effect. We now consider the case in which the backscattered fluorescence from the close-field region is negligible in comparison with that for the far-field region. This consideration is well justified, in the first approximation, because the nonradiative transfer rate due to the interaction between the atomic evanescent wave of the excited atom and the surface is larger than the spontaneous-emission rate. We assume that the excited atoms are completely de-energized in the near-field region without radiation.

Thus from Eqs. (1), (6), and (12) we obtain the desired result, while keeping in mind that a backscattered photon emitted in the far field can be lost by self-absorption in the close-field region:

$$L_{eg}^{f}(\nu_L) = F_{\nu_L} Y_{eg} \Gamma(-\mathbf{n}_L) \alpha_{ge}(\nu_L) \exp[-\overline{\tau_{ge}^{f}}(\nu_L)] \times \int_{\Delta\nu} \frac{\alpha_{eg}(\nu)}{\alpha_{ge}(\nu_L) + \alpha_{ge}(\nu)} \exp[-\overline{\tau_{ge}^{f}}(\nu)] \mathrm{d}\nu. \tag{13}$$

In the next subsection we use this equation to theoretically evaluate the influence of the ratio ϵ on the shape of the integrated retrofluorescence signal.

3. Simulation of the Backscattered-Fluorescence Intensity

For purposes of illustration it is useful to simplify Eq. (13) and examine the effect of the interaction between atoms and the conductive surface of the cell. We assume that the line shapes for far-field and near-field regions are the same. The normalized integrated radiance is given by

$$L_{eg}^{n}(\nu_L) = S(\nu_L) \exp[-pS(\nu_L)] \int_{\Delta\nu} \frac{S(\nu)}{S(\nu_L) + S(\nu)} \times \exp[-pS(\nu)] \mathrm{d}\nu, \tag{14}$$

where $p = \overline{\tau_{ge}^{f}}(0)$ is the effective optical thickness evaluated to zero detuning and $S(\nu)$ is a distribution function. As an example, for a Lorentzian distribution, $S(\nu)$ may be written

$$S(\nu_L) = \left\{ 1 + \left[\frac{2(\nu_L - \nu_0)}{\Delta\nu_{\mathrm{Lor}}} \right]^2 \right\}^{-1}, \tag{15}$$

where $\Delta\nu_{\mathrm{Lor}}$ is the full width (FWHM) of the Lorentz line and ν_0 is the center of the line.

To estimate the filtering effect on retrofluorescence, we consider hypothetical atomic vapor, having $S(\nu)$ as a Lorentzian distribution, with $\Delta\nu_D = 1$ GHz. We evaluate the integrated backscattered-fluorescence for different values of p (Fig. 2). The curve at $p = 0$ presents the in-

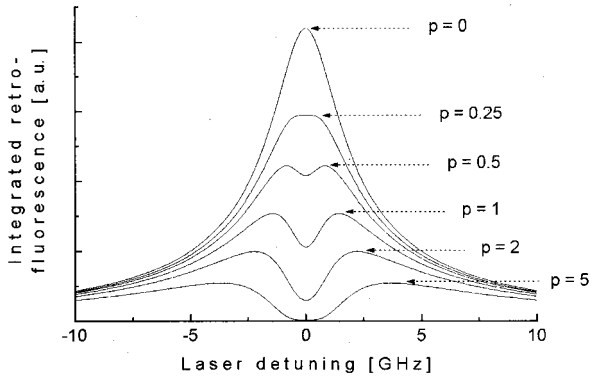

Fig. 2. Simulated integrated retrofluorescence signal as a function of laser detuning from the resonance line center around resonance for different values of the effective optical thickness (p).

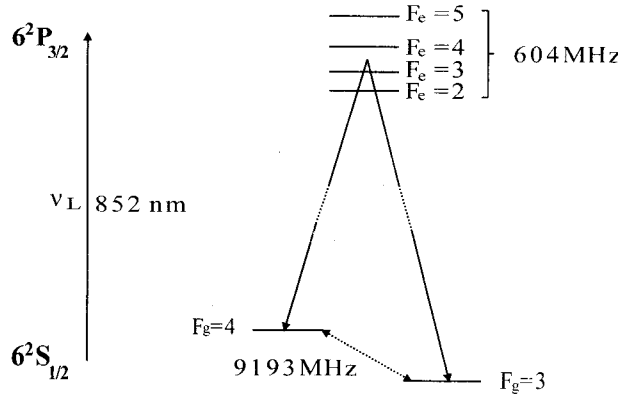

Fig. 3. Energy-level diagram corresponding to the $6^2S_{1/2}$–$6^2P_{3/2}$ line of a cesium atom. The energy gaps are not to scale.

tegrated retrofluorescence without surface effects. As expected, a reversal of the line is not obtained with only the self-absorption effect. The dip begins for $p > 0.28$ and increases rapidly. For $p = 1$, the inhibition represents a loss of 75% from the signal without surface effects. Using Eq. (1), for $p = 2$, we have only 14% of the laser intensity passing through the filter region. Finally, if $p > 2$, it is difficult to get spectroscopic information from the far- and near-field regions at line center taking into account the approximations used.

B. Application to the Transition Cs 852.2 nm

In formulating our model we have to consider the hyperfine structure for the absorption transition Cs [$6^2S_{1/2} \rightarrow 6^2P_{3/2}$]. In Fig. 3 we have a schematization of these hyperfine levels for the terms Cs $6^2S_{1/2}$ and $6^2P_{3/2}$. These atomic terms are composed of two hyperfine ground levels Cs $6^2S_{1/2}(F_g = 3$ or 4) energetically isolated from each other by a gap of 9.193 GHz and four excited lying–hyperfine levels $6^2P_{3/2}$ ($F_e = 2$, 3, 4, or 5) over a spectral interval of 604 MHz. Considering both the collisions and the distribution of kinetic energy in the vapor, it is reasonable to assume, in our case, a complete redistribution of the excited population. In this case we obtain a new formula cross section for the filter reduced to the simple form

$$\sigma^f_{F_g \rightarrow F_e}(\nu_L) = \frac{\lambda^2}{8\pi}\frac{(2J_e + 1)}{(2J_g + 1)} g_{F_eF_g}\epsilon_{F_eF_g}A^f_{J_e \rightarrow J_g}\alpha^f_{F_g \rightarrow F_e}(\nu_L), \quad (16)$$

where $g_{F_eF_g}$ is equal to

$$g_{F_eF_g} = \frac{(2F_e + 1)(2F_g + 1)}{(2I + 1)}\{\ldots 6j \ldots\}^2. \quad (17)$$

I is the spin of the nucleus, $\{\ldots 6j \ldots\}$ represents the symbol $6j$, F_e and F_g are the hyperfine quantum number of the excited and ground levels, respectively, and $\alpha^f_{F_g \rightarrow F_e}(\nu_L)$ is the normalized shape for each hyperfine line. If the bandwidths of excited hyperfine structure overlap, the spectral-absorption cross section is principally determined by the excited hyperfine structure. For the ground levels, which are well isolated from each other, the effective spectral-absorption cross section is given by adding the contribution of the various hyperfine transitions. Thus

$$\sigma^f_{F_g \rightarrow J_e}(\nu_L) = \sum_{F_e} \sigma^f_{F_g \rightarrow F_e}(\nu_L) = \frac{\lambda^2}{8\pi}\frac{(2J_e + 1)}{(2J_g + 1)} A^f_{J_e \rightarrow J_g}\sum_{F_e} \epsilon_{F_eF_g} g_{F_eF_g}\alpha^f_{F_g \rightarrow F_e}(\nu_L). \quad (18)$$

In this case the optical thickness becomes

$$\overline{\tau^f_{F_g \rightarrow J_e}}(\nu_L) = \sum_{F_e} \overline{\tau^f_{F_g \rightarrow F_e}}(\nu_L) = \sigma^f_{F_g \rightarrow J_e}(\nu_L)\overline{n_{F_g}}\,\overline{x_f}, \quad (19)$$

$$\overline{k^f_{F_g \rightarrow J_e}}(\nu_L) = \sigma^f_{F_g \rightarrow J_e}(\nu_L)\overline{n_{F_g}}, \quad (20)$$

where $\overline{n_{F_g}}$ is the effective density of hyperfine ground level F_g. Finally, with an overlapping of the ground hyperfine level, the optical thickness of the filter will be reduced to the form

$$\overline{\tau^f_T}(\nu_L) = \sum_{F_g}\sum_{F_e} \overline{\tau^f_{F_g \rightarrow F_e}}(\nu_L). \quad (21)$$

As for the filter equation, we modify the equation of retrofluorescence taking account of the hyperfine structure in the far field. We consider $\alpha_{F_e \rightarrow F_g}(\nu) = \alpha_{F_g \rightarrow F_e}(\nu)$.

So, setting the normalized function $\alpha_T(\nu)$,

$$\alpha_T(\nu) = \sum_{F_g}\sum_{F_e} g_{F_eF_g}\alpha_{F_e \rightarrow F_g}(\nu), \quad (22)$$

we obtain the following formula of the total integrated retrofluorescence with surface effects:

$$L^f_T(\nu_L) = F_{\nu_L}Y_{J_eJ_g}\Gamma(-\mathbf{n}_L)\alpha_T(\nu_L)\exp[-\overline{\tau^f_T}(\nu_L)] \times \int_{\Delta\nu} \frac{\alpha_T(\nu)}{\alpha_T(\nu_L) + \alpha_T(\nu)}\exp[-\overline{\tau^f_T}(\nu)]\mathrm{d}\nu. \quad (23)$$

Since the hyperfine structure is well known, this last equation will be used in the parametric study of the experimental integrated backscattered spectra in Section 6.

4. EXPERIMENTAL SETUP

The setup diagram is presented in Fig. 4. The cesium vapor is excited by a frequency modulated beam of an EOSI laser diode (model LCU 2001 M) with a bandwidth smaller than 10 MHz. We choose the lines of the hyperfine structure $[6^2P_{3/2}(F_e = 3, 4, 5)-6^2S_{1/2}(F_g = 4)]$ and $[6^2P_{3/2}(F_e = 2, 3, 4)-6^2S_{1/2}(F_g = 3)]$ at 852.2 nm. The laser does a frequency sweep around this bandwidth and is protected from the return signal by an isolator. A part of the laser beam is sent through a Fabry–Pérot interferometer that allows scaling of the explored spectral band. In order to maintain thermal isolation, the Pyrex cesium cell is embedded in a metallic covering, leaving only the windows open. This is placed on a MIRAK thermometer (model HP 72935) at a programmable temperature under a Pyrex cover. A uniform temperature throughout the cell is obtained. The beam is directed to the entrance cell window at an angle of ~2° with reference to the normal at the surface. The frequency-modulated (FM) selective-reflection spectrum is observed with a Si photodiode. The total backward radiation (backscattered, nonresonance backscattering, and light from energy-pooling collisions), captured at an angle of ~16° with reference to the normal, is focused onto the adjustable entrance slit of a monochromator Jarrell–Ash (model 5) that is equipped with a photomultiplier. The spectral retrofluorescence signal from the monochromator exit slit of the monochromator is amplified by a picoampere meter (Keithley Instruments). The signals are then digitalized and sent to the computer. The spectral sweeping step of the laser is adjustable. For the study of the spectrum at low resolution of retrofluorescence on a bandwidth of 660 GHz (22 cm^{-1}) we use an exploration stepping of 2.1 GHz (0.07 cm^{-1}). For the study of the spectrum at high resolution associated with the hyperfine structure of the ground level covering a bandwidth of 20 GHz, we use a fine piezoelectrical sweeping with a resolution of a few MHz. We limit ourselves to weak laser powers (100 μW) for a beam area of ~0.014 cm^2. At higher laser powers, the retrofluorescence spectrum has spectral properties that are different from the previous case. These spectral properties most likely result from complex nonlinear effects.

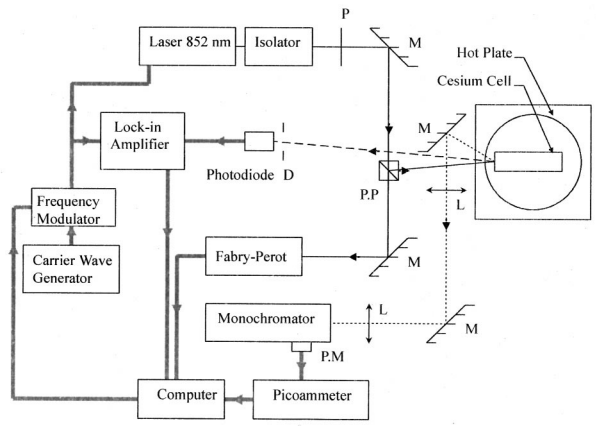

Fig. 4. Experimental setup: P, polarization rotator; L, lens; M, mirror; P.P, polarizing prism; P.M., photomultiplier; D, spatial filter.

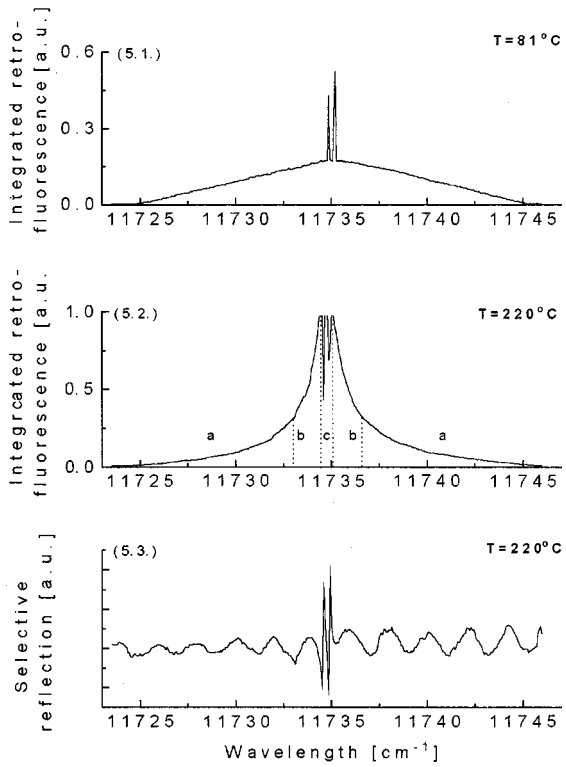

Fig. 5. Laser scanning through a wide band centered on the $6^2P3_{/2}-6^2S_{1/2}(F_g = 3, 4)$ resonance lines with a laser power of 100 μW: (5.1.) Integrated fluorescence signal at $T = 81\,°C$. (5.2.) Integrated fluorescence signal at $T = 220\,°C$ with (a) vapor considered as optically thin, (b) vapor where the laser beam is strongly attenuated, and (c) very optically thick vapor. (5.3.) Selective-reflection signal at $T = 220\,°C$.

5. EXPERIMENTAL RESULTS

We first present the integrated retrofluorescence spectrum at spectral line 852.2 nm for different temperatures. These data are then completed by a measurement of the nonresonant atomic line emission at 917.2 nm excited by the effect of energy-pooling transfer. Finally, preliminary results in correspondence with the molecular spectrum Cs_2 are obtained.

A. Retrofluorescence Spectrum at 852.2 nm ($6^2P_{3/2}-6^2S_{1/2}$)

The integrated retrofluorescence signal measurement, induced at the interface by the diode laser beam sweeping a wide spectral band, is presented in Fig. 5 for cell temperatures of 81 °C and 220 °C.

The integrated retrofluorescence spectrum in Fig. 5.1 is taken at a temperature cell of 81 °C to determine the instrumental function of the monochromator. The cesium vapor, which is completely crossed by the laser beam, shows that the region is optically thin and that the signal shapes for two hyperfine resonant lines are well resolved. We note the presence of a very wide spectrum of half-width of 11.3 cm^{-1} on the very narrow spectral resonant hyperfine transitions $6^2P_{3/2}-6^2S_{1/2}(F_g = 4, 3)$. We attribute a large part of the observed spectrum to the nonresonant interaction with the glass surface (diffusion). The width of the entrance slit of the monochromator be-

ing equal to that of the exit slit, we note that in this case the spectral instrumental function is triangular. Figure 5.2 presents the spectral backscattered signal for a cell at a temperature of 220 °C. The central region of the signal is truncated to see more clearly the detailed edges of the signal. We subdivide the spectral bandwidth into three sections (a), (b), and (c) characterized by some distinctive features.

Section (a). This section corresponds to the optically thin, or almost transparent, vapor at these frequencies. We attribute a large part of the observed signal to a nonresonant backscattered laser beam in a glass window. The intensity of the signal is limited by the instrumental function of the monochromator. As backscattered light is not frequency selective, the interface behaves like a nonresonant diffuser in this spectral band.

Section (b). In this section there is a retrofluorescence signal with a wide spectral bandwidth close to 140 GHz (4.67 cm^{-1}). The laser beam passing through an absorbing layer of thickness smaller than the geometric dimension of the cell is strongly attenuated in the vapor, which gradually becomes optically thick as we approach section (c). A large proportion of the atoms excited at level $6^2P_{3/2}$ by the laser beam are close to the entrance window of the cell. The majority of the atoms nevertheless stay relatively far ($>\lambda$) from the surface window, and the interaction with the surface on the excited state $6^2P_{3/2}$ of the vapor is not yet evident. The instrumental function of the monochromator, which is very large, plays no role in the profile of the retrofluorescence hyperfine spectrum. The depopulating of the excited state $6^2P_{3/2}$ by the spontaneous-emission processes and the energy-pooling collisions (the excitation of higher levels by inelastic collisions between $6^2P_{3/2}$ excited atoms) make an important contribution to the emerging light in this spectral bandwidth. The energy-pooling collisions process is easily observable by the study of the atomic emission lines from the UV to the near-IR.

Section (c). The most important section of the spectral bandwidth close to 15 GHz is associated with a large value of the optical thickness of the absorbing vapor layer, particularly at the center of the resonance line. We consider that the laser radiation is completely absorbed in a very thin vapor layer compared with that of section (b). Figure 5.2 reveals an intense backscattered-fluorescence inhibition signal corresponding to the two-hyperfine resonant transitions at 852.2 nm. Figure 5.3 shows a recording of the selective-reflection spectrum for the same spectral bandwidth as the preceding case (Fig. 5.2). The centers of the selective-reflection lines and the centers of the inhibiting lines are almost completely superimposed in the first approximation. The small visible modulations on this spectrum are attributed to a Fabry–Pérot residual effect at the cell window. Laser energy, which is lost by reflection, cannot explain the inhibition of the retrofluorescence signal at the center of each hyperfine line.

Figure 6 shows section (c) in greater detail for three different temperatures (134 °C, 180 °C, and 220.6 °C) for a bandwidth laser sweeping of 20 GHz. As the preceding case, the simultaneous measurement of the FM selective-reflection spectrum shows that the deep dips in the retrofluorescence spectrum correspond, in the first approximation, to the center of the two lines associated with the hyperfine structure of the ground state $6^2S_{1/2}$. For different measuring conditions depending on the temperature cell (<150 °C) we observe a sub-Doppler hyperfine structure in the deep dips of the retrofluorescence spectrum. A more detailed study of this hyperfine structure observed for the first time with the retrofluorescence spectroscopy method will be presented in the near future.

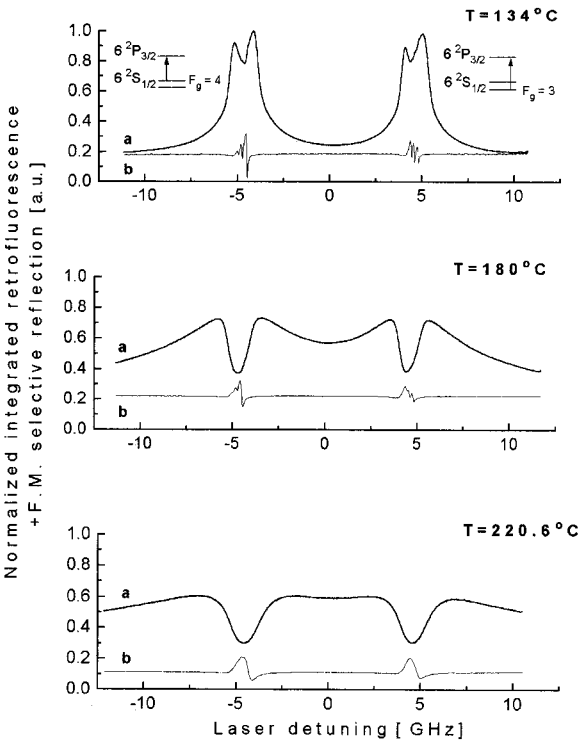

Fig. 6. (a) Integrated retrofluorescence spectrum at 852.2 nm as a function of the laser detuning for different temperatures. The observed asymmetries in the dip deep shapes are produced by the sub-Doppler effect and the statistical weight of the hyperfine components of the $6^2P_{3/2}$ level. (b) Corresponding FM selective-reflection spectrum.

B. Fluorescence at 917.2 nm ($6^2D_{5/2}$–$6^2P_{3/2}$)

In order to check our assertion, namely, that energy lost at the boundary is not converted by energy-pooling nonresonant settlement in excited levels, we consider a transition that is connected to level $6^2P_{3/2}$. The optical pumping of the $6^2P_{3/2}$ population can generate a rich atomic Cs spectrum by the effect of energy-pooling collisions (inelastic collisions). The population in the high-lying levels results from collisions between excited atoms in which the two atoms involved pool their internal energy to produce both ground and higher excited-state atoms. The strong nonresonant 917.2 nm ($6^2D_{5/2}$–$6^2P_{3/2}$) line invokes the higher $6^2D_{5/2}$ state that is mostly populated by 6^2P binary collisions. The integrated spectral intensity of this line with the monochromator adjusted to the 917.2-nm line is shown in Fig. 7 with a scanning laser tuned near the 852.2-nm line. The spectral signal at 157 °C is observed under the same experimental conditions as the spectra of Fig. 6. There is also a dip in the center of the 917.2-nm lines generated by the energy-pooling effect when the laser is tuned to the bandwidth of

the resonant hyperfine structure at the 852.2-nm lines. The disappearance of the energy-pooling effect when the laser pumping is tuned to the center of the atomic resonance line can only be interpreted by a strong depopulating mechanism of the excited level $6^2P_{3/2}$. All the atomic lines analyzed due to the energy-pooling effect manifest the same behavior. More details on this spectrum will be presented soon.

C. Cs_2 Molecular Fluorescence

Before concluding, we want to check the reduction of the molecular fluorescence signal when the laser is tuned to a resonance. The emission spectrum of the dimers indirectly originates from the nonelastic collisions between the excited cesium atoms. The atoms excited by collisions emit radiations that are partially absorbed by the dimers. Therefore it is reasonable to suppose that the Cs_2 band spectrum at 780 nm originates from the photon relaxation to the $8S_{1/2}$ state excited by $6P$–$6P$ energy-pooling collisions. A second process consists of the creation of dimers in collisions between two excited atoms (7^2D–6^2S, 8^2D–6^2S, 6^2D–6^2S, 8^2S–6^2P, 9^2S–6^2S, 8^2P–6^2S, and 6^2P–6^2P). These collisions create ionized dimers that cause a radiative cascade when recombining with an electron. The presence of spectral Cs_2 bands is therefore linked to the populating of the cesium's excited states. A spectrum corresponding to the dimers bands attributed to the $X\ ^1\Sigma_g^+$–$B\ ^1\Pi_u$ transition is shown in Fig. 8. The top spectrum is observed when the laser is tuned to the wing of the 852.2 nm line. The identified atomic lines are superimposed on the molecular spectrum. For the bottom spectrum the laser is tuned to the center of the 852.2-nm resonance. By comparing the two measurements, one notices a disappearing of the Cs_2 emission band and a significant reduction of 760-nm and 794-nm atomic line intensities. When the laser is tuned to the resonance frequency, both the Cs_2 band spectrum and the atomic line inhibition are consequences of the disappearance of the $6^2P_{3/2}$ excited atoms in the vapor by a nonradiative mechanism.

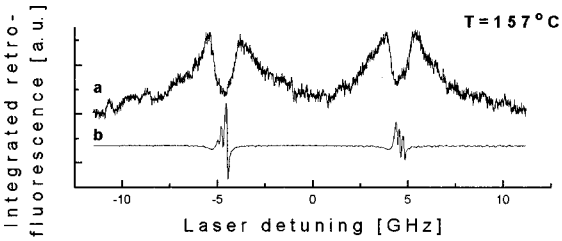

Fig. 7. (a) Integrated retrofluorescence signal [a.u.] at the 917.2-nm line ($6^2D_{5/2}$–$6^2P_{3/2}$) due to the energy-pooling effect as a function of the laser detuning from the 852.2-nm resonance line. (b) Corresponding FM selective-reflection spectrum at 852.2 nm [a.u.].

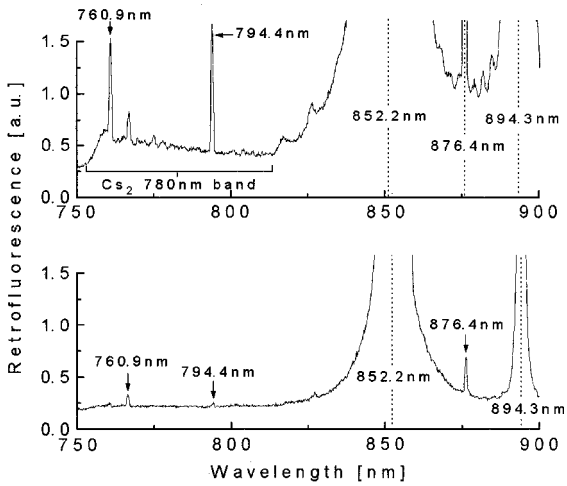

Fig. 8. Atomic and molecular fluorescence spectra with, on the top, the laser tuned in the wings of the 852.2-nm resonance line and, on the bottom, the laser tuned in the center of this resonance line.

6. PARAMETRIC COMPARISON BETWEEN THEORY AND EXPERIMENTAL RESULTS

We use Eq. (23) to calculate the parameter $A^f_{J_e \to J_g}$ with a fit. The temperatures are chosen as a function of their correspondence with the model. Indeed, at lower temperatures (<150 °C) the total redistribution hypothesis on the excited level is probably not justified. Following Subsection 3.A.3, we also have an upper limit for T. We arbitrarily limit its value to $T \leqslant 200\,°\mathrm{C}$.

As an example, we present our parametric results for a temperature of 155.4 °C. The absorption shape of each component of the excited-state hyperfine structure is taken into account. The shapes of the absorption lines in the far-field region are Voigt profiles. The Doppler and Lorentzian widths of each component in this region are fixed at 452.5 MHz and 97.2 MHz, respectively. It is difficult to predict the absorption shape in the filter region, so we leave it as a floating parameter.

The other atomic parameters are $\lambda = 852.2\,\mathrm{nm}$, $A_{J_e \to J_g} = (1/3) \times 10^8$, $J_e = 3/2$, $J_g = 1/2$, and $\overline{n}\,(T = 155.4\,°\mathrm{C}) = 2.63 \times 10^{14}\,\mathrm{atoms\,cm^{-3}}$.

Figure 9 shows that our theoretical result is totally consistent with the experimental spectrum. It gives, in our case, a ratio of $\tilde{\epsilon}_{F_g=4} \approx 29$ and $\tilde{\epsilon}_{F_g=3} \approx 44.6$ ($\tilde{\epsilon}_{F_g}$ being the effective ratio between nonradiative and radiative transfer rates for a transition J_e–F_g), depending on the nature of surface. At higher temperatures, parametric fits give a lower value for ϵ. This variation could be attributed to a shielding effect by excited atoms close to the surface. As the atomic density increases, the dipole in the remote region of the filter cannot completely see the surface. Alternatively, with a constant effective ratio ϵ for the atoms closest to the surface, the geometrical depth of the filter decreases. Parametric fits also show that absorption in the near field does not respect the statistical weight rules between hyperfine transitions. Those discrepancies must be clarified, and we need a more extended analysis of these data.

7. CONCLUSIONS

An experiment has been carried out with a laser-diode power of 100 μW, with a spectral bandwidth less than 10 MHz, tunable throughout the Cs 852.2 nm ($6^2P_{3/2}$–$6^2S_{1/2}$) hyperfine spectrum to study simultaneously retrofluorescence and selective-reflection spectra

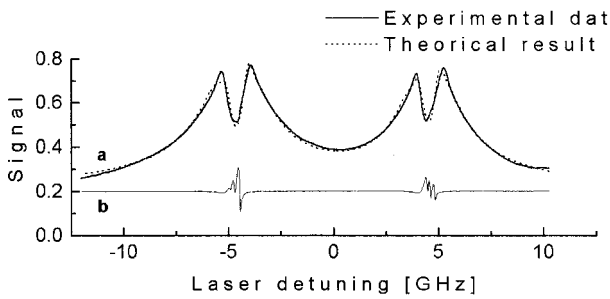

Fig. 9. (a) Comparison of the normalized integrated retrofluorescence signal between experimental and theoretical spectra calculated from Eq. (23). (b) Corresponding experimental FM selective-reflection signal [a.u.].

at the glass–vapor interface. Integrated retrofluorescence has been experimentally characterized for a 852.2-nm resonance line, a 917.2-nm nonresonant line generated by energy-pooling collisions $6P–6P$, and Cs_2 molecular spectra at high Cs density between 10^{13} and 10^{15} at. cm^{-3}. An integrated backscattered inhibition signal has been observed when the laser diode is tuned in the center of the 852.2-nm hyperfine lines. We have examined the processes that can influence the retrofluorescence hyperfine spectrum: self-absorption, the combined effect of radiation and migration of excitation transfer at the interface, and interaction between atomic evanescent waves and the dissipative surface. A simple mathematical model has been developed for the integrated backscattered hyperfine fluorescence. We have considered the boundary as separated into two distinct regions: a wavelength-thickness vapor layer where the excited atoms interact strongly with the dissipative surface and a more remote region where the atoms are insensitive to the presence of a surface. Experimental results are compared with the prediction made by use of the model. They are consistent and give a value of the effective nonradiative transfer rate in the near field for the excited level $6^2P_{3/2}$ of the order of $1.17 \times 10^9\ s^{-1}$. It will be interesting to compare this rate with that of $6^2P_{1/2}$ and 7^2P states. A similar study with Rb is planned. We need more theoretical information on nonradiative energy-transfer results from the coupling of a large number of excited atoms to the dissipative surface, particularly to estimate the possibility of a screening effect of a conductive surface.

Other spectroscopic methods for analyzing the annihilation photon in the near-field region may be considered. In particular, a method based on the observation of Cs_2 dimers destruction at the ground state in the presence of an excited $6^2P_{3/2}$ population[19] would probably allow characterization of the filtering effect. A second method based on optogalvanic spectroscopy is being explored in order to study this effect at the cell interface. Preliminary results are promising. The sub-Doppler structure observed in the dip of the lines is now being analyzed. We have characterized, for the first time to our knowledge, an original and accurate method for clarifying and understanding an old spectroscopic problem related to the nature of glass–metallic vapor interfaces.

ACKNOWLEDGMENTS

This research was funded in part by the Natural Sciences and Engineering Research Council of Canada. The expert technical assistance of P. A. Dion and Y. Lemire is gratefully acknowledged. We are grateful to S. Levesque for helpful comments.

REFERENCES

1. M. Fichet, F. Schuller, D. Bloch, and M. Ducloy, "Van der Waals interactions between excited-state atoms and dispersive dielectric surfaces," Phys. Rev. A **51**, 1553–1564 (1995).
2. V. Vuletic, V. A. Sautenkov, C. Zimmermann, and T. W. Hänsch, "Optical pumping saturation effect in selective reflection," Opt. Commun. **108**, 77–83 (1994).
3. V. Vuletic, V. A. Sautenkov, C. Zimmermann, and T. W. Hänsch, "Measurement of cesium resonance line self-broadening and shift with Doppler-free selective reflection spectroscopy," Opt. Commun. **99**, 185–190 (1993).
4. M. Oria, M. Chevrollier, D. Bloch, M. Fichet, and M. Ducloy, "Spectral observation of surface-induced Van der Waals attraction on atomic vapour," Europhys. Lett. **14**, 527–532 (1991).
5. M. Chevrollier, D. Bloch, G. Rahmat, and M. Ducloy, "Van der Waals-induced spectral distortions in selective-reflection spectroscopy of Cs vapor: the strong atom–surface interaction regime," Opt. Lett. **16**, 1879–1881 (1991).
6. V. A. Sautenkov, A. M. Akul'shin, and V. L. Velichanskii, "Selective reflection-method of intradoppler spectroscopy of optically dense gaseous media," J. Appl. Spectrosc. **50**, 189–192 (1989).
7. M. F. H. Shuurmans, "Spectral narrowing of selective reflection," J. Phys. (France) **37**, 469–485 (1976).
8. M. A. Bouchiat, J. Guéna, Ph. Jacquier, M. Lintz, and A. V. Papoyan, "Electrical conductivity of glass and sapphire cells exposed to dry cesium vapor," Appl. Phys. B **68**, 1109–1116 (1999).
9. A. G. Zajonc and A. V. Phelps, "Nonradiative transport of atomic excitation in Na vapor," Phys. Rev. A **23**, 2479–2487 (1981).
10. J. M. Wylie and J. E. Sipe, "Quantum electrodynamics near an interface," Phys. Rev. A **30**, 1185–1193 (1984).
11. R. R. Chance, A. Prock, and R. Silberg, "Comments on the classical theory of energy transfer," J. Chem. Phys. **62**, 2245–2253 (1975).
12. D. G. Hummer and P. B. Kunasz, "Migration of excitation in transfer of spectral line radiation," J. Quant. Spectrosc. Radiat. Transfer **16**, 77–96 (1976).
13. A. F. Molisch, B. P. Oehry, and G. Magerl, "Radiation-trapping in a plane parallel slab," J. Quant. Spectrosc. Radiat. Transfer **48**, 377–396 (1992).
14. R. D. Cowan and G. H. Dieke, "Self-absorption of spectrum lines," Rev. Mod. Phys. **20**, 418–455 (1948).
15. Y. C. Chao, L. S. O. Johansson, and R. I. G. Uhrberg, "Layer growth of Cs on Si(100)$c(4 \times 2)$ studied with photoelectron spectroscopy," Phys. Rev. B **56**, 15446–15451 (1997).
16. N. V. Smith, "Optical constants of rubidium and cesium from 0.5 to 4.0 eV," Phys. Rev. B **2**, 2840–2849 (1970).
17. I. I. Sobel'man, *Introduction to the Theory of Atomic Spectra*, International Series of Monographs in Natural Philosophy (Pergamon, Oxford, 1972), Vol. 40, p. 297.
18. J. B. Taylor and I. Langmuir, "Vapour pressure of caesium by the positive ion method," Phys. Rev. **51**, 753 (1937).
19. M. Lintz and M. A. Bouchiat, "Dimer destruction in a Cs vapor by a laser close to atomic resonance," Phys. Rev. Lett. **80**, 2570–2773 (1998).